Discover Materials

RESEARCH Open Access

Quaternised cellulosic materials prepared from chain-growth polymerisation of a grafted reactive ionic liquid

Muzamil Jalil Ahmed[1], Baohu Wu[2] and Antoni Sánchez-Ferrer[1*]

*Correspondence:
Antoni Sánchez-Ferrer
sanchez@hfm.tum.de
[1]Wood Materials Science, Wood Research Institute of Munich (HFM), TUM School of Engineering and Design, Technical University of Munich, 80797 Munich, Germany
[2]Jülich Centre for Neutron Science (JCNS) at Heinz Maier-Leibnitz Zentrum (MLZ), Forschungszentrum Jülich, 85748 Garching, Germany

Abstract

Grafting-onto modified cellulosic materials using reactive ionic liquids (RILs) is emerging as a green and versatile strategy to tailor surface chemistry and functionality. This paper investigates the process–structure–property relationships of quaternised celluloses using glycidyltriethylammonium chloride (GTEAC) as a RIL, and microfibrillated cellulose (MFC) and nanocrystalline cellulose (NCC) as core materials. The resulting quaternised materials, QMFC and QNCC, exhibited distinct chemical and structural changes confirmed by FTIR, SEM/EDX, and WAXS/SAXS. The chain-growth polymerisation of GTEAC on MFC or NCC led to a substantial reduction in crystallinity, or an increase in the amorphous content (QMFC: from 85% to 54%; QNCC: from 82% to 60%), while the crystalline domains remain intact. Moreover, grafting increased the intercrystallite spacing (QMFC: from 4.3 to 5.8 nm; QNCC: from 3.7 to 5.0 nm), indicating that the poly-GTEAC chains intercalate in the amorphous domains and between crystallites. Thermal analyses (TGA/DSC) demonstrated that grafted materials start decomposing at lower temperatures (QMFC: from 283 °C to 133 °C; QNCC: from 281 °C to 142 °C). Dynamic vapour sorption (DVS) studies showed that equilibrium moisture uptake at a_w = 0.95, as well as the monolayer capacity and the specific surface area values, nearly doubled. Notably, QNCC exhibited superior grafting efficiency and sorptive performance due to its high surface-to-volume ratio.

Keywords Reactive ionic liquid, Glycidyltriethylammonium chloride, Cellulose, Graft polymerisation, Process-structure-property

1 Introduction

The abundance of cellulose and its purported utility, economics, biodegradability, and versatility in material applications have been relatively offset by its poor surface chemistry [1, 2]. This renders the ease of functionalisation for native cellulose as critically challenging for developing high-value derivatives for such as composites, functional materials for separation processes [2, 3], packaging materials [4, 5], and biomedical surfaces [6]. Cellulose functionalisation, more specifically, in the context of hydrophilisation, typically requires chemical modification, which can be material-, cost- and

energy-intensive. Graft polymerisation stands out as a promising technique to introduce desired functionalities while maintaining the native cellulose core chains intact, i.e., heterogeneous modifications [7, 8]. Such reactions often necessitate the use of copious amounts of organic solvents, which are known to be hazardous to health, flammable, and volatile [9]. These concerns, therefore, catalyse a push towards greener, safer liquid media for such reactions, i.e., ionic liquids (ILs).

Traditional nitrogen-containing ILs based on R-methylimidazolium [Rmim], R-pyridinium [Rpy], R-methylpyrrolidinium [Rmpyrro], R-methylmorpholinium [Rmmor] and R-methylpiperidinium [Rmpip] cationic units – where R = alkyl - have been used extensively for cellulose dissolution – actually, stable dispersions - and grafting applications, reducing reliance on hazardous organic solvents [9]. Even though ILs are considered to be unreactive, under certain conditions, they can behave as Brønsted acids, as active catalytic species or as nucleophilic anions [10]. These ILs offer an interesting approach to solubilise and functionalise cellulose simultaneously or, at least, partake in the functionalisation as a catalyst with the cost of some degree of cleavage of the cellulose chains [11]. Missoum et al. reported a heterogeneous surface modification of native cellulose with different C1 to C6 anhydrides using [bmim][PF_6] as a liquid medium [12]. Zhang et al. reported a reactive extrusion process to heterogeneously modify cellulose using [bmim][Cl] and phthalic anhydride, maleic anhydride and butyl glycidyl ether – leveraging a high shear stress of the extruder to dissolve and react cellulose [13]. However, in such techniques, processing complexity and overuse of solvents and/or reagents are staggering.

When the R-moeity on the IL is a reactive group, e.g., vinylic functionality [14, 15], the grafting-onto strategy using the so-called reactive ionic liquids (RILs) involves covalent attachment of polymerisable IL units directly onto cellulose surfaces [16]. This approach offers several key advantages over pre-formed polymer grafting, including higher graft density control, improved interfacial contact, retained morphological structure, and reduced use (and even recyclable) of solvents [17]. The occurrence of self-polymerising RILs is scarcely reported, and their use for cellulose grafting is even scarcer. This necessitates the need for a one-pot, single liquid medium – a polymerisable RIL (poly-RIL) – that is both reactive and assists in effective cellulose functionalisation, independent of cellulose dissolution.

In earlier works, we have demonstrated the use of glycidyltriethylammonium chloride (GTEAC) as an epoxy-based quaternary ammonium RIL for quaternising cellulosic materials such as pinewood [8] and microfibrillated cellulose [7]. The method involves a solventless reaction at elevated temperature (> 120 °C), where a portion of the poly-RIL could be recycled. This methodology mitigates solvent waste, avoids extreme pH values, and ensures high purity (~ 94%), making it well-suited for sustainable grafting applications. Contemporary research uses a similar quaternisation agent, i.e., glycidyltrmethylammonium chloride (GTMAC) or 3-chloro-2-hydroxypropyltrimethylammonium chloride (CHPTAC), as aqueous alkaline solutions [18, 19]. The use of these reagents, albeit common, is marred by a substantial over-hydrolysis of the amorphous cellulose domains that adversely affect the native cellulose structure. Furthermore, the use of aqueous media can lead to decomposition of the glycidyl-based RILs [20]. By comparison, GTEAC serves as both a reaction medium due to its liquid nature and as a reactive monomer because of the epoxy reactive moiety, enabling chain-growth polymerisation

directly at the cellulose surface/interface, forming polycationic brushes and entangled fibres [7, 8]. This simplifies processing, improves grafting efficiency, and enhances control over the resulting polymer architecture. This feature is critical in inducing electrochemical, ion-exchanging, as well as other functional properties to the cellulosic material [19–21].

In this work, we use the solvent-free semi-dry kneading method under inert conditions, therefore, avoiding the hydrolysis of the RIL and the cellulosic material, minimising solvent usage, maximising interfacial contact, and resulting in uniform grafting distribution [22, 23]. We further compare the impact of the grafting process on microfibrillated cellulose (MFC), which is semicrystalline, and nanocrystalline cellulose (NCC). Cellulosic materials vary in morphology and surface characteristics, which strongly influence grafting behaviour [2, 24]. These distinct morphologies allow us to investigate how the substrate structure affects GTEAC grafting density, in terms of degree of quaternisation DQ, degree of crystallinity, and functional performance. Herein, we demonstrate that GTEAC-grafting introduces cationic polyelectrolyte brushes that intercalate between the crystallites of cellulose and penetrate the amorphous domains. The study attempts to establish the relationships between: (1) processing (graft protocol); (2) structure (crystallinity, intercrystallite spacing and correlation lengths); and (3) property (thermal behaviour and moisture sorption). Therefore, the present work serves to provide a template for green, high-value cellulose derivatives using RILs under solvent-minimised protocols.

2 Materials and methods

2.1 Materials

Microfibrillated cellulose (MFC) – Celova® C500 (length: 0.5–1.6 mm; 32 µm size) – was provided by Weidmann Fiber Technology AG (Switzerland). Celluforce NCC™ (NCC) nanocrystalline was purchased from CelluForce (Canada), comprising cellulose sulphate sodium salt (0.7 g/cm^3, 44–108 nm length, 2.3–4.5 nm diameter, 70 nm hydrodynamic radius, 0.86–0.89% S content). All other ancillary chemicals were procured from Merck kGaA (Germany). Deuterium oxide (D_2O) with a deuterium content of 99.9% was acquired from VWR Avantor (Germany).

2.2 Methods

2.2.1 Synthesis of the RIL

The glycidyl triethylammonium chloride (GTEAC) monomer was synthesised as described in an earlier work by Ahmed and Sánchez-Ferrer [8]. The purity of the GTEAC was 94% (according to the ^{1}H NMR analysis provided in the paper). The synthesis of the GTEAC is shown in Scheme 1a.

2.2.2 Grafting onto and functionalisation of cellulosic materials using the RIL

The functionalised cellulose materials, i.e., quaternised microfibrillated cellulose (QMFC) and quaternised nanocrystalline cellulose (QNCC), have been prepared using MFC and NCC, respectively. The quaternisation and chain-growth polymerisation have been performed with the "*semi-dry kneading method*", described in an earlier work by Ahmed et al. [7]. The molar ratio between the GTEAC and the cellulose's repeating unit, i.e., the anhydroglucose unit (AGU) or the sodium sulphate anhydroglucose unit

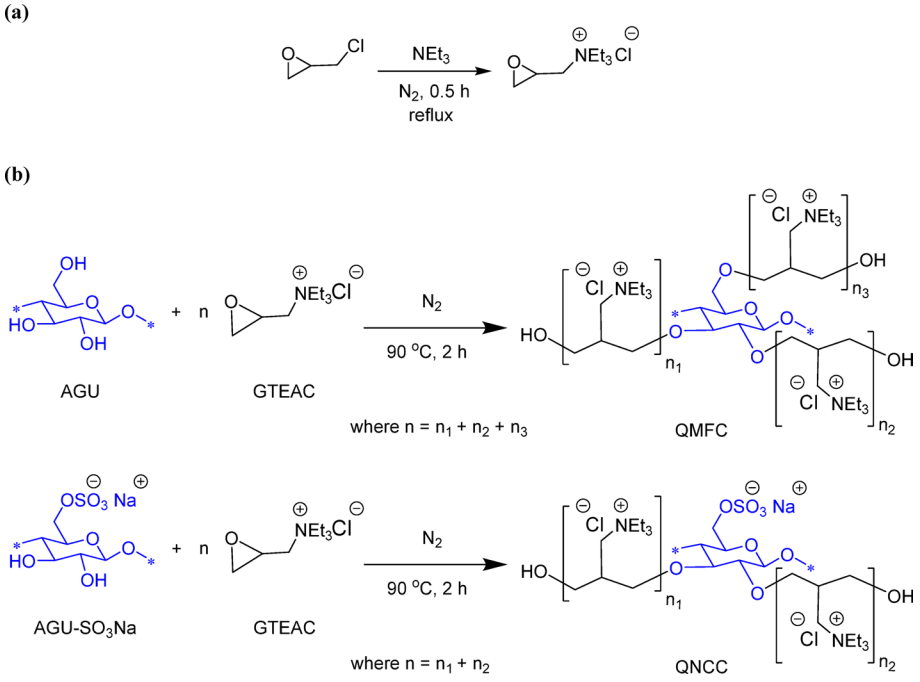

Scheme 1 Reaction scheme for (**a**) GTEAC and (**b**) quaternised cellulosic materials, e.g., QMFC and QNCC. Note: AGU and AGU-SO_3Na, anhydroglucose and sodium sulphate anhydroglucose unit; GTEAC, glycidyltriethylammonium chloride

(AGU-SO_3Na), was 12:1. The reaction was performed at 90 ℃ for 2 h under an inert atmosphere. The grafting-onto procedure is indicated in Scheme 1b. The resulting materials were washed thoroughly with deionised water to remove the excess reactants and decomposates until a clear filtrate was obtained. All functionalised materials were dried at 80 ℃ for 1.5 h. The post-grafting characteristics of these materials have been defined using the weight gain (w_g) and the degree of quaternisation (DQ), calculated as follows:

$$w_g = \frac{w - w_0}{w_0} \times 100\% \tag{1}$$

$$DQ = \frac{w - w_0}{w_0 \cdot M_{GTEAC}} \tag{2}$$

where w_0 and w are the dry mass of the pre- and post-grafting cellulosic materials, e.g., QMFC and QNCC. The RIL, i.e., GTEAC, molar mass M_{GTEAC} amounts to 193.72 g/mol.

2.2.3 Chemical and morphological analysis

Fourier-transform infrared (FTIR) spectra were recorded using a Nicolet iS50 spectrophotometer (ThermoFisher Scientific, USA) with an attenuated total reflection (ATR) accessory (diamond/ZnSe crystal). Spectra were recorded in the range of 4000–600 cm^{-1}, at a spectral resolution of 4 cm^{-1} and averaged over 64 scans. The D_2O-exchanged FTIR experiments were also performed to determine spectral peaks of functional groups other than those of absorbed water. The D_2O-exchanged FTIR-ATR procedure is briefly described in an earlier work by Ahmed et al. [7].

Scanning electron microscopy (SEM) images were recorded with a Carl Zeiss EVO-40 XVP (Germany) for microstructural and morphological analysis. Moreover, Energy-dispersive X-ray (EDX) analysis was performed in low vacuum (~0.01 Pa) with an accelerating voltage of 15 kV at 97× magnification. The EDX experiments were conducted to identify the elemental composition of all materials and, therefore, the presence of functional groups across the samples' microstructure.

2.2.4 Thermal analysis

Thermogravimetric analysis (TGA) experiments were performed using a TGA50/M3 from Mettler Toledo (Switzerland) and controlled by a TC15 TA controller from Mettler Toledo (Switzerland). TGA experiments were conducted in standard Al_2O_3 crucibles from 25 to 1000 ℃ at a heating rate of 10 K/min under an inert atmosphere. Differential scanning calorimetry (DSC) experiments were carried out on a DSC 822 calorimeter from Mettler Toledo (Switzerland) with an autosampler. 5 mg samples were placed in a 40 µL perforated aluminium pan. The DSC was taken from − 50 ℃ to 500 ℃ at a heating rate of 10 K/min under an inert atmosphere.

2.2.5 Structural analysis

Small-angle X-ray scattering (SAXS) and wide-angle X-ray scattering (WAXS) experiments were performed using a Xenocs XUESS 3.0 XL KWS-X (France). The scattering patterns were obtained using a high flux Excillum Metal-Jet D2 + X-ray source (Sweden) featuring a liquid metal anode (250 W; 70 kV; 3.57 mA) with $\lambda_{GaK\alpha}$ radiation of 0.1314 nm. The X-ray scattered intensity was collected using a Dectris 2D Eiger2R 4 M X-ray detector (Switzerland) of 15.5 cm (width) × 16.3 cm (height) and 75 µm resolution, and with a sample-to-detector distance from 0.1 m to 1.70 m. An effective scattering vector range of 0.05 $nm^{-1} < q < 45$ nm^{-1} was obtained, where q is the scattering wave vector ($q = 4\pi\sin\theta/\lambda$). The degree of crystallinity (χ) was calculated by the deconvolution of the WAXS signal into crystalline and amorphous peaks in the WAXS patterns, the areas of which give the $\chi = A_{crystalline}/(A_{crystalline} + A_{amorphous})$ [25–28]. The SAXS intensity profiles were fitted using a pseudo-Voigt peak function that allowed for the evaluation of the scatterers' distance (D) and the correlation length (ξ).

2.2.6 Dynamic vapour sorption

Dynamic vapour sorption (DVS) experiments were conducted as described by Sánchez-Ferrer et al. [29], using the Surface Measurement Systems gravimetric DVS Advantage ET (UK) vapour sorption device. The device comprises a microbalance and a N_2-purged chamber with a 200 cm^3/min (12 L/h) flow rate at a selected relative humidity (RH). Samples were initially conditioned at 25 ℃ and 0% RH until completely dry. Measurement starts with the increase in RH of the N_2 flow in steps of 5% until ~ 100% RH (adsorption). The RH is cycled back (desorption), reducing in steps of 5% until 0% RH. The criterion for change in RH is related to $d(m/m_0)/dt < 0.001\%$/min over 10 min; at this point, the sample is measured for one extra hour before changing the RH for the next measuring step. Each dynamic moisture sorption step was analysed using the double stretched exponential (DSE) model [29], and the extrapolated values were used to construct the corresponding moisture sorption isotherms and fitted using the modified Guggenheim, Anderson, and de Boer (GAB) model [30, 31]. The sorption site occupancy

(SSO) model was implemented to evaluate the number of binding sites per mass of the sample [32, 33].

3 Results and discussion

3.1 Grafting-onto and functionalisation of cellulosic materials using the RIL, GTEAC

The grafting-onto method considers all available OH groups in the amorphous domains and in the crystallite surface of the cellulosic material. The GTEAC monomer undergoes a ring-opening polymerisation whereby it reacts with the OH from the AGU and AGU-SO_3Na to first form a triethylammonium 2-hydroxypropyl (TEAHP) group. This group can further react with another GTEAC monomer and undergo chain-growth polymerisation to form cationic polyelectrolytes, i.e., poly-GTEAC [8]. This method is sensitive to moisture as the GTEAC monomer can decompose into water-soluble decomposates containing quaternary ammonium enolates [8, 20]. This, therefore, requires that an anhydrous, inert environment is maintained during the semi-dry kneading process. The grafting-onto method yields a weight gain of $38.5\% < w_g < 41.4\%$ or a quaternisation degree of $2.04 < DQ < 2.13$ mmol/g for the QMFC and QNCC. These values conform to what has been observed for the GTEAC-modified cellulosic materials in earlier studies [7, 8]. A challenge associated with this GTEAC chain-growth polymerisation is that the increasing number of cationic polyelectrolytes grafted onto the cellulosic materials causes aggregation, and flocculation or precipitation in aqueous and non-aqueous dispersions alike. For this reason, NMR measurements were impractical to perform instantaneously.

3.2 Chemical Functionalisation, Surface, morphological and elemental analysis

3.2.1 Chemical functionalisation

The chemical functionalisation of the post-grafting cellulosic materials, i.e., QMFC and QNCC, has been investigated using FTIR-ATR and compared to the reference starting materials, i.e., MFC and NCC, respectively, in order to prove the grafting process. Fig. 1 shows the characteristic absorption peaks consistently observed across the two types of quaternised cellulose materials, i.e., 3335 (ν, C–OH), 2979 (ν, $–CH_3$), 2890 (ν, –CH–), 1640 (ν, absorbed H_2O), 1480 (ν, C–N from poly-GTEAC), 1440–1350 (δ, –CH from AGU), 1030 (ν, C–O–C), and 1150–950 cm^{-1} (ν, C–O), as well as the peaks at 1255 (ν, RO-SO_3^-) and 790 cm^{-1} (ν, S-O) for the sulphate containing cellulosic materials. The quaternisation process is, therefore, confirmed by the presence of the CN peak across spectra compared to that of the poly-GTEAC. NCC typically has a similar surface area (400 m^2/g) to microfibrillated cellulose (500 m^2/g), which allows for an efficient functionalisation [34]. Notably, peaks associated with the TEAHP group are stronger in the QNCC, owing to a higher surface area available during the quaternisation and chain-growth GTEAC polymerisation process. Alternatively, the mobility of the amorphous regions of QMFC influences H-bonding between networks, which can further contribute to higher peak intensities than QNCC [35]. D_2O-exchanged samples clearly indicate the presence of absorbed water across all cellulosic materials (1640 cm^{-1}), which is evidently more prominent for QMFC and QNCC in contrast to their original materials. This relative increase in absorbed water is owed to the increased hydrophilicity of the grafted cellulosic materials [7, 20, 34]. In general, the peaks associated with the cellulose chains, i.e., CO and COC, remained essentially the same.

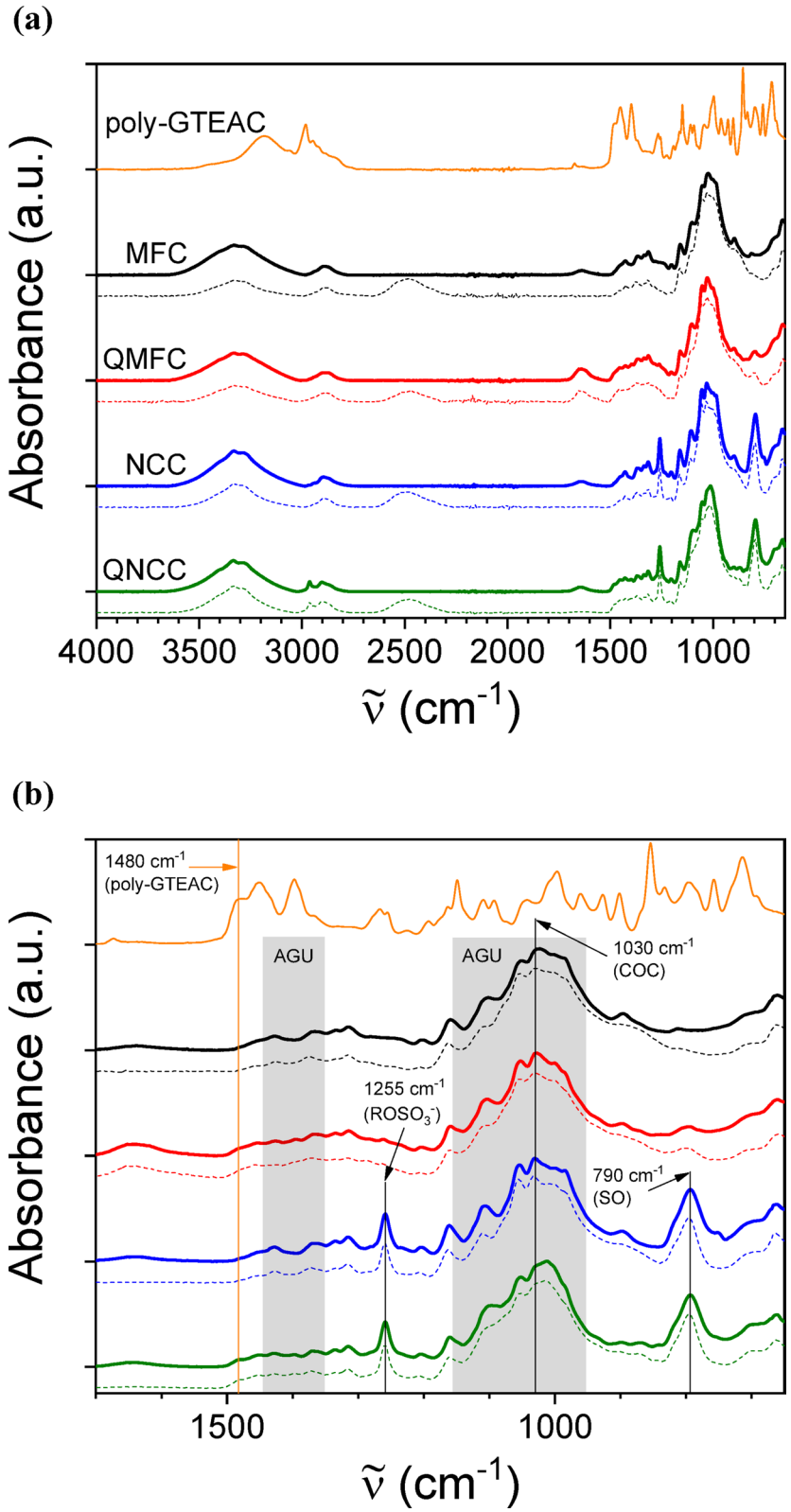

Fig. 1 (**a**) FTIR-ATR spectra for the poly-GTEAC (orange), MFC (black), QMFC (red), NCC (blue) and QNCC (green) in bold lines. D_2O-exchanged spectra are indicated in similar colours but with dashed lines. (**b**) Zoom region from 1700 to 650 cm^{-1} indicating the most relevant absorption peaks

3.2.2 Surface, morphological and elemental analysis

The surface and morphological features were further examined using scanning electron microscopy (SEM) for the pre- and post-grafted cellulosic materials (MFC, NCC, QMFC and QNCC). Further, the chemical (elemental) analysis was performed using SEM/EDX. The technique allows for the semi-quantitative determination of N from the quaternary ammonium (NEt_3^+) groups and Cl^- as the counter-ions from the grafted poly-GTEAC. The SEM images for the pre-grafted cellulosic materials, i.e., MFC and NCC, indicate typical fibre bands and granules/crystallites of cellulose aggregates, respectively (Fig. 2a and c). Moreover, the evidence of grafted polymers is observable in both QMFC and QNCC samples, as shown in Fig. 2b and d, though more extensively in the latter. There is a distinct increase in the surface roughness marked by a waxy surface (Fig. 2b), indicating coverage by amorphous material, i.e., the poly-GTEAC. Similarly, for QNCC, there is a significant transition from a granulated NCC texture to visibly waxier, platelet-like microstructures (Fig. 2d).

In general, the SEM images indicate the formation of aggregated/flocculated structures in the QMFC and the QNCC samples, owing to the entanglement caused by the cationic polyelectrolytic chains [36]. The corresponding EDX analyses indicate for both the QMFC and QNCC samples the presence of N (k_α = 0.392 keV) and Cl (k_α = 2.622 keV, k_β = 2.816 keV). Additional peaks observed in the EDX analyses correspond to the k_α emissions of impurities having Al (k_α = 1.486 keV) and Si (k_α = 1.740 keV), as well

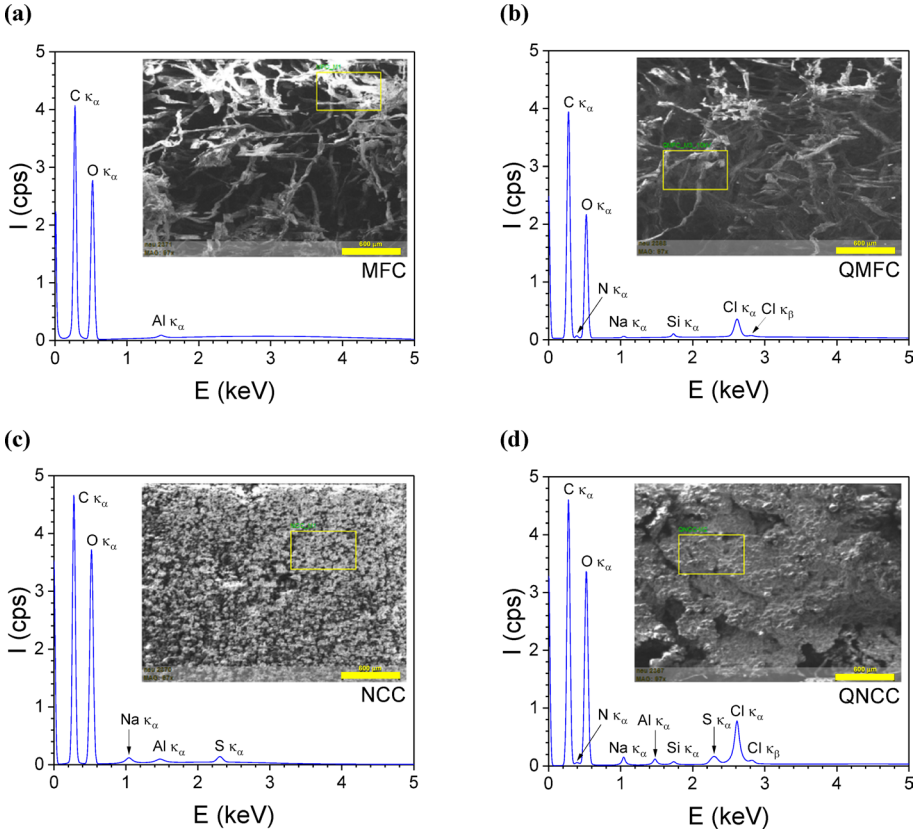

Fig. 2 SEM-EDX analysis for the (**a**) MFC, (**b**) QMFC, (**c**) NCC and (**d**) QNCC samples. The insets are SEM micrographs, and the scale bars correspond to 600 µm

as Na (k_α = 1.041 keV) and S (k_α = 2.307 keV) in samples containing sodium sulphate groups, i.e., NCC and QNCC.

3.3 Structural properties

Scattering experiments (WAXS and SAXS) were performed to investigate any potential structural changes in the crystallite assembly or, more specifically, in the dispersion of the crystalline domains within the amorphous matrix. An extensive WAXS analysis is shown in Fig. 3a-d for the pre- and post-grafted cellulosic materials (MFC, NCC, QMFC and QNCC). The described quaternisation process, "*semi-dry kneading method*", does not incur substantial changes to the original structure of the cellulose crystalline domains. In other words, the original monoclinic cellulose I allomorph is retained, having lattice parameters of $a = 0.8$ nm, $b = 0.8$ nm, $c = 1.03$ nm, and $\gamma = 96.3°$. The crystalline peaks' shape (blue curves) allowed for the estimation of the cellulose crystallite's dimensions in terms of average length (l), width (d) and thickness (h). These values have been tabulated in Table 1. In general, the crystallite dimensions are relatively consistent after the quaternisation process, indicating no change in the crystalline domains.

SAXS characterisation for MFC and QMFC (Fig. 4a and b) indicates a significant shift of the broad peak (q) from 1.5 nm^{-1} to 1.1 nm^{-1}. This shift corresponds to an increase in the lateral distance between the crystalline domains (D), indicating that the grafted poly-GTEAC chains act to 'push apart' the individual crystalline domains by swelling the amorphous domains. Similarly, the correlation length (ξ) between these crystallites

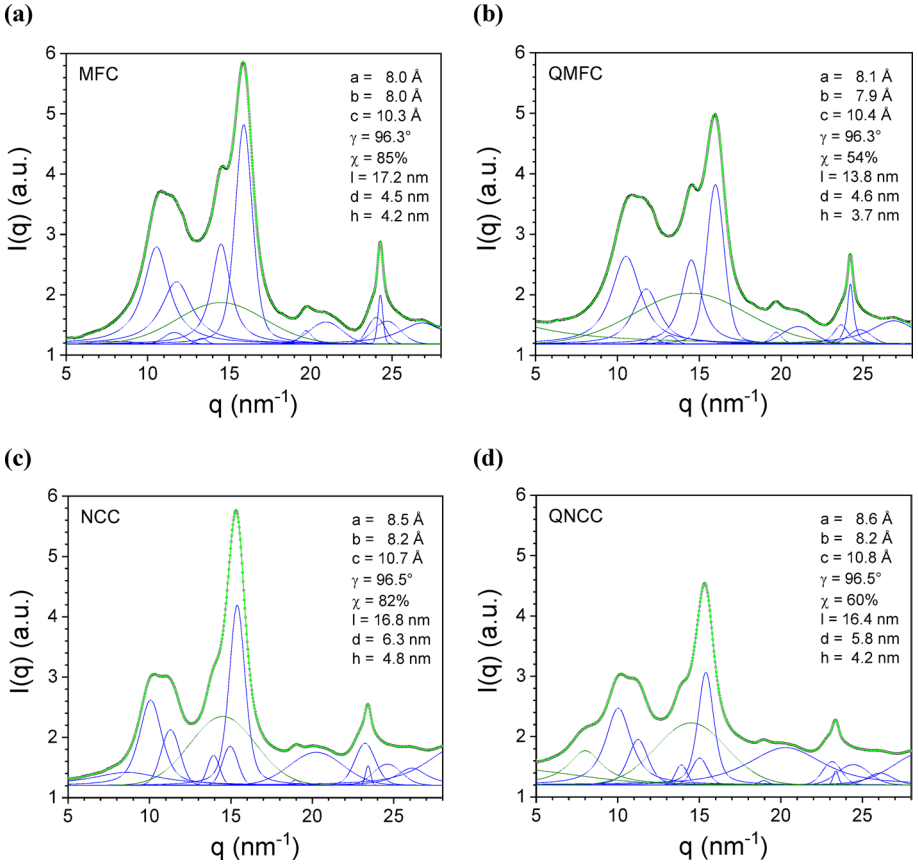

Fig. 3 WAXS profiles for the **a**) MFC, **b**) QMFC, **c**) NCC and **d**) QNCC samples. The light green curves represent the fit to the experimental data by deconvolution into the crystalline (blue) and amorphous (green) peaks

Table 1 Lattice parameters (a, b, c and γ), the degree of crystallinity (χ), the average dimensions of the cellulose single crystal (l, d and h), the lateral distance between crystallites (D) and correlation length (ξ) obtained by WAXS and SAXS analysis

Sample	a (Å)	b (Å)	c (Å)	γ (deg)	χ (%)	l (nm)	d (nm)	h (nm)	D (nm)	ξ (nm)
MFC	8.0	8.0	10.3	96.3	85	17.2	4.5	4.2	4.3	3.6
QMFC	8.1	7.9	10.4	96.3	54	13.8	4.6	3.7	5.8	5.5
NCC	8.5	8.2	10.7	96.5	82	16.8	6.3	4.8	3.7	4.4
QNCC	8.6	8.2	10.8	96.5	60	16.4	5.8	4.2	5.0	4.7

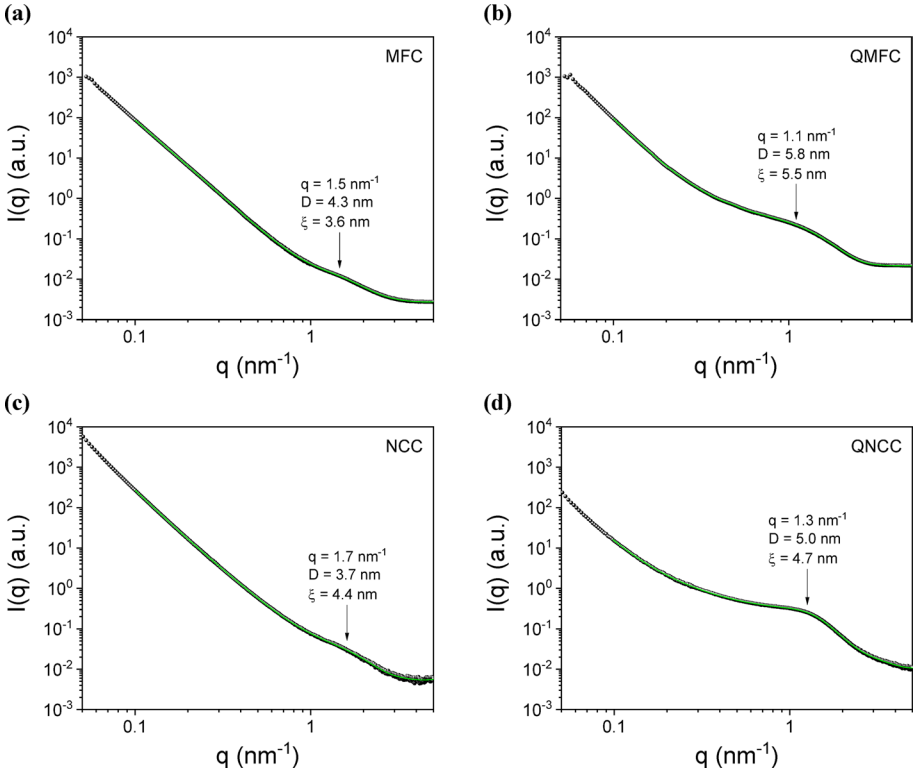

Fig. 4 SAXS profiles for the **a**) MFC, **b**) QMFC, **c**) NCC and **d**) QNCC samples. The light green curves represent the fit to the experimental data

moves from 3.6 to 5.5 nm, even though both crystalline domains remained randomly distributed and embedded within the amorphous matrix. In contrast, for NCC and QNCC, the broad peak shift occurs from 1.7 nm^{-1} to 1.3 nm^{-1}, corresponding to a lateral distance from 3.7 to 5.0 nm (Fig. 4c and d). Additionally, while the presence of poly-GTEAC does indicate a similar effect in the increase of later distances as for the case of the MFC/QMFC, the effect is not so prominent due to the lack of cellulose amorphous domains between crystallites.

As shown in Fig. 4, an increase in D and ξ, more pronounced in QMFC than QNCC, suggests that polymer chains intercalate more freely in the MFC matrix. This disparity can be attributed to greater amorphous flexibility in MFC versus the densely packed NCC. The parameters from the SAXS analysis are also presented in Table 1. Finally, the degree of crystallinity (χ) was determined from the WAXS patterns, as the ratio between the area of all the deconvoluted crystalline peaks (blue curves) with respect to the total area of the scattering signal (green curve). The results indicate a loss in crystallinity owing to the increasing inclusion of amorphous content, i.e., the poly-GTEAC, in both

Table 2 Water peak (T_w), water percentage (m_w) and water endset temperature (T_{end}), onset decomposition temperature (T_{on}), maximum decomposition temperature (T_{max}), local decomposition temperatures (T'_{max} and T''_{max}), and residual mass at 1000 °C $(m/m_0)_{end}$. Obtained from the TGA analysis

Sample	T_w (°C)	m_w (%)	T_{end} (°C)	T_{on} (°C)	T'_{max} (°C)	T_{max} (°C)	T''_{max} (°C)	$(m/m_0)_{end}$ (%)
MFC	50	4.20	151	283		355		5.3
QMFC	50	7.55	116	133	158	340	306	0.4
NCC	52	4.08	151	281		302	350	0
QNCC	50	4.26	130	142	159	288	390	0

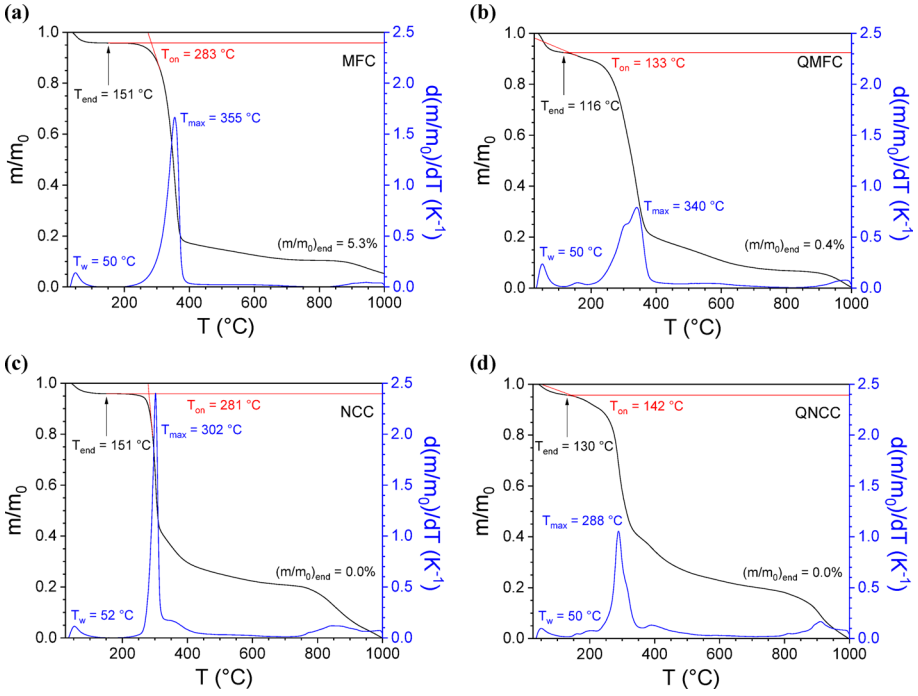

Fig. 5 TGA thermograms (black) together with the corresponding derivative curves (blue) for the (**a**) MFC, (**b**) QMFC, (**c**) NCC and (**d**) QNCC samples

the QMFC and QNCC samples. This loss in χ corresponds to a change from 85% (MFC) to 54% for QMFC, and from 82% (MFC) to 60% for QNCC after poly-GTEAC grafting. In NCC, which is composed of rigid, highly crystalline nanorods with fewer internally accessible amorphous regions, the grafting occurs predominantly as a surface coating on some of the six rectangular lateral faces, and on the two hexagonal faces that are prone to becoming amorphous. So the crystalline core remains largely intact and the reduction in χ is correspondingly smaller (Δχ = 22%) than for MFC (Δχ = 31%).

3.4 Thermal properties

Thermogravimetric analyses (TGA and DTG) of the pre- and post-grafed cellulosic materials were performed to ascertain their thermal stability (from 25 °C to 1000 °C) and to quantify the absorbed moisture. Results are described in Table 2. Further, Fig. 5a and b show the TGA/DTG thermograms of MFC and QMFC, where a three-step decomposition for the post-grafted sample can be observed, involving: (1) moisture loss, (2) early decomposition of the amorphous domains, i.e., amorphous cellulose and poly-GTEAC

chains, and (3) crystalline cellulose polymer backbone degradation. Further, a slight decrease in the maximum thermal decomposition (T_{max}) for the former is observed at 355 °C for MFC to 340 °C for the QMFC. These decomposition temperatures correspond to those observed for native glucopyranose chains in cellulose [37, 38]. Similarly, in Fig. 5c and d, for NCC and QNCC, a larger difference is observed where the T_{max} drops to 288 °C from 302 °C.

Notably, the presence of the grafted cationic polyelectrolytes, the poly-GTEAC, tends to lead to an earlier onset decomposition temperature T_{on}, for QMFC (133 °C) and QNCC (142 °C) compared to the corresponding pre-grafted cellulosic materials, i.e., MFC (283 °C) and NCC (281 °C), respectively. The degradation is aggravated by the presence of propylene glycol-based polymers such as the poly-GTEAC grafted onto cellulose with bulky or flexible side chains [39, 40]. This disrupts the crystalline structure of cellulose and typically lowers thermal stability and decomposition onset. The DTG signal for QMFC and QNCC indicates additional decomposition peaks at 158 °C and 159 °C, which are likely attributable to the grafted poly-GTEAC. Ahmed and Sánchez-Ferrer demonstrated in an earlier study that a model grafted substrate of poly-GTEAC decomposed at 223 ℃ [8]. The grafted poly-GTEAC, in this case, has a lower T'_{max} owing to a lower degree of polymerisation, in contrast to the model polymer with a degree of polymerisation of n = 13. The other local, late-stage decomposition peak associated with the still-degrading glucopyranose chain is observed at 306 °C, 350 °C and 390 °C for QMFC, NCC and QNCC, respectively.

The temperatures associated with the water loss process T_w and T_{end}, for QMFC, indicate a 7.6% (vs. 4.2% for MFC) water loss and QNCC a slightly higher water loss by 4.3% (vs. 4.1% for NCC). The increase in water loss is attributed to the increased hydrophilicity of the post-grafted cellulosic materials and the capability of the microstructure to retain more water. The latter feature is prominent for fibrous materials, where the water molecules are easier to trap in the cellulose fibrils, their entangled web-like structures that prevent total water loss [41, 42]. This is not the feature of nanocrystalline cellulosic materials, which feature more rigid, granulated or rod-like structures [43].

Figure 6 shows the DSC thermograms of the pre- and post-grafted cellulosic materials. The pre-grafted cellulosic materials, MFC and NCC, demonstrate a single significant endothermic peak at 369 °C and 311 °C, respectively. This endothermic peak is related to the decomposition of the cellulose chain [37]. Comparatively, the QMFC and QNCC exhibit glass transitions at 56 °C (Δc_p = 0.114 J/(g·K)) and 55 °C (Δc_p = 0.084 J/(g·K)), respectively. These findings correspond to what has been observed for other cellulosic materials grafted using GTEAC [7, 8]. The decomposition occurs earlier for the QMFC and QNCC at 272 °C and 277 °C, respectively, associated with the poly-GTEAC grafted amorphous cellulose domains. The decrease in the decomposition temperatures indicates the grafting of the thermolabile poly-GTEAC that lowers thermal stability, i.e., an increase of amorphous content of the native cellulosic material. QMFC shows an additional decomposition event at 363 °C corresponding to later decomposition stages of grafted residual polysaccharides containing more ordered cellulose fractions. The grafting onto is further demonstrated by comparing the decrease in the heat capacity of the T_g of the QMFC and QNCC with that of the model grafted polymer investigated in an earlier work [8], i.e., T_g = 8 ℃ and Δc_p = 0.350 J/(g·K).

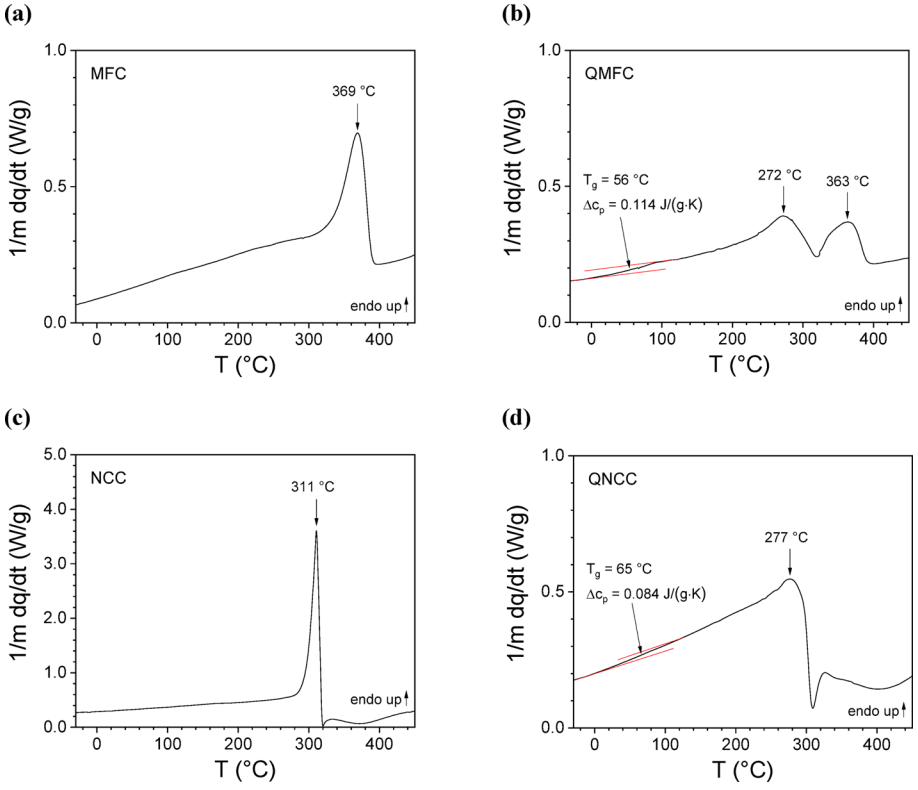

Fig. 6 DSC thermograms for the **a**) MFC, **b**) QMFC, **c**) NCC and **d**) QNCC samples

3.5 Water sorption behaviour

The water sorption behaviour of the pre- and post-grafted cellulosic materials was studied using DVS, by analysing the moisture content of the samples as a function of the water activity or relative humidity (a_w = RH/100). Moisture sorption isotherms were analysed using a modified Guggenheim–Anderson–de Boer (GAB) model [29, 31]. The model accurately fits multilayer sorption isotherms in the water activity range of $0 < a_w < 0.99$, and allows for the evaluation of the monolayer moisture content and specific surface area. The model is given by:

$$\mathrm{EMC} = \frac{\Delta m}{m_0} = \frac{MC_0 \cdot C \cdot K \cdot a_w}{(1 - K \cdot a_w)(1 + (C-1)K \cdot a_w)} + \frac{MC_0 \cdot C \cdot K \cdot N \cdot a_w^2}{(1 - K \cdot a_w)(1 - a_w)} \quad (3)$$

where Δm is the water mass uptake, m_0 is the dry mass of the sample at $a_w = 0$, MC_0 is the monolayer moisture content capacity, and C, K and N are the GAB fitting parameters. The Sorption Site Occupancy (SSO) model is based on the number of sorption sites available [32], assuming proton-active moieties that bind water molecules, such as –OH groups in cellulose [44, 45]. The model is given as follows:

$$M_{SSO} = M^0_{SSO} \cdot a_w^n \quad (4)$$

where M_{SSO} is the moisture capacity corresponding to the bound water molecules to the sorption sites, M^0_{SSO} is the maximum amount of bound water, and n is the exponent. The fitting parameters for the GAB and SSO models are listed in Table 3 for the pre- and post-grafted cellulosic materials.

Table 3 GAB parameters (MC_0, C, K and N), SSO parameters (M^0_{SOO}, n and a^*_w), and hysteresis factor (η) obtained from the DVS analysis

Sample	MC_0 (g/g)	C	K	*N* (mol/g)	M^0_{SSO} (g/g)	*n*	a^*_w	η
MFC	0.048	10.5	0.721	0.002	0.080	0.50	0.191	1.16
QMFC	0.077	10.8	0.793	0.002	0.142	0.53	0.186	0.99
NCC	0.053	8.5	0.735	0.005	0.089	0.55	0.188	1.18
QNCC	0.105	1.6	0.686	0.029	0.125	0.99	0.071	1.02

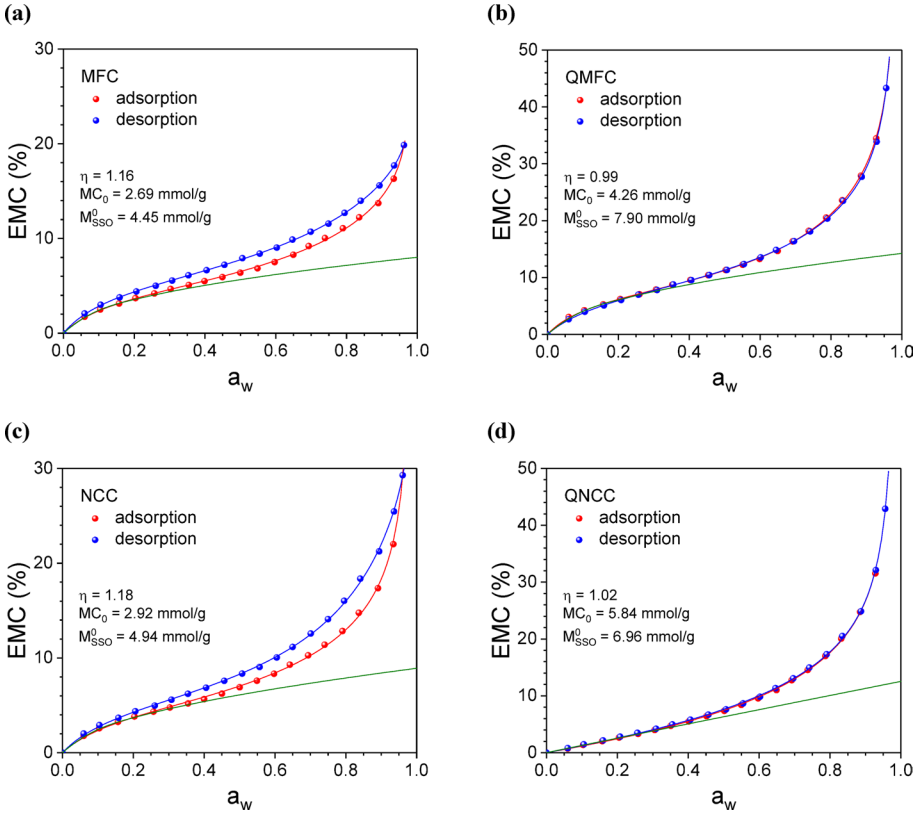

Fig. 7 DVS moisture sorption isotherms for the **a**) MFC, **b**) QMFC, **c**) NCC and **d**) QNCC samples, together with the adsorption (red) and desorption (blue) GAB fitting curves and the SSO fitting curve (green). Note: EMC is the Equilibrium Moisture Content (%)

Figure 7 shows the DVS curves for the pre- and post-grafted cellulosic materials, where the distinct S-shape is evident between the adsorption/desorption curves. The MFC and NCC have a hysteresis factor of 1.16 and 1.18, respectively. However, post-grafting hysteresis is negligible for QMFC and QNCC, showing an almost ideal reversible sorption phenomenon, as $\eta \approx 1$, due to the presence of the amorphous grafted poly-GTEAC.

Furthermore, the equilibrium moisture content (EMC) value is higher for the QMFC (ca. 41%) than the MFC (ca. 18%) at a_w = 0.95. For QNCC, a similar trend is observed, i.e., ca. 40% compared to the ca. 26% for NCC. The higher retention of water pertains to the presence of amorphous, hydrophilic, cationic polyelectrolytes, i.e., the poly-GTEAC grafted chains and the remaining proton-active hydroxyl moieties on the cellulose crystallite surface and in the amorphous cellulose domains [7].

The monolayer moisture content MC_0 increases significantly for the post-grafting materials, i.e., from 2.69 mmol/g (MFC) to 4.26 mmol/g (QMFC) and from 2.92 mmol/g

(MFC) to 5.84 mmol/g. Similarly, the bound water moisture capacity M^0_{SSO} for the pre- and post-grafted cellulosic materials shows an overall increase from the former to the latter. For instance, from 4.45 mmol/g (MFC) to 7.90 mmol/g (QMFC), and from 4.94 mmol/g (NCC) to 6.96 mmol/g (QNCC).

Finally, the specific surface area SSA for the pre- and post-grafted cellulosic materials was estimated from the GAB model [30], using:

$$SSA = \frac{MC_0 \cdot N_A \cdot \sigma}{m_0 M_w} \tag{5}$$

where N_A, m_0, σ and M_w correspond to Avogadro's number (6.022×10^{23}), the dry mass of the sample, the cross-sectional area and the molecular weight of a water molecule, i.e., 0.125 nm^2 and 18.01 g/mol, respectively. The SSA values for the MFC increase substantially upon grafting with the hydrophilic cationic polyelectrolytes, i.e., from 184 m^2/g to 292 m^2/g. This post-grafting effect is more prominent for the NCC, for instance, NCC increases from 201 m^2/g to 401 m^2/g for QNCC. Similarly, the increase in MC_0 and M^0_{SSO} corroborates the presence of poly-GTEAC chains in the post-grafted cellulosic material. This further owes to the reduced structural collapse, which allows for water retention, as observed elsewhere for polymer grafts to cellulose microcrystals [46].

3.6 Process-Structure-Property relations

Grafting onto cellulose surfaces enhances the availability of functional groups, allowing for increased quaternisation that contributes to the overall surface area accessible for water retention [47]. The interdependence of processing parameters, resulting micro-/nanostructure, and macroscopic properties is central to tailoring quaternised cellulosic materials for advanced applications. In terms of the process element, a 12:1 molar ratio of GTEAC/AGU ensures an excess of reactive epoxy groups, driving high grafting density (or the DQ ≈ 2.0–2.1 mmol/g). Maintaining an inert, moisture-free atmosphere during the 2 h of reaction at 90 °C, the kneading step avoids premature monomer hydrolysis and promotes efficient chain-growth polymerisation of surface-bound species [7, 8]. Mechanical mixing under semi-dry conditions facilitates close contact between cellulose fibrils/crystallites and the RILs, leading to uniform surface coverage [23]. This contrasts with solution-based methods that often yield heterogeneous graft distributions or entangled polymer agglomerates together with the hydrolysis of the cellulose-based materials as well as extensive reagent/material input loss during processing [12].

In terms of the structure element, results demonstrate a conversion of smooth fibrillar or rod-like cellulose to "waxy" coatings indicative of amorphous poly-GTEAC brushes or entangled fibre-like networks. The polymer grafts act as intercalants and preferentially populate amorphous interstices and crystallite surfaces. A similar trend has been observed by Harrisson et al. in the case of cellulose microcrystals grafted with amine-terminated polyaromatics and polyalkylacrylates [46]. Such changes in the structure manifest in significant changes in the properties of the post-grafted cellulosic material. For instance, lower decomposition temperatures are owed to the thermolabile quaternary ammonium moieties disrupting cellulose H-bonding and facilitating early chain scission [48]. The poly-GTEAC, therefore, can form a brush-like microstructure that extends into the surrounding medium, increasing the effective particle volume and external surface area [7]. This improves interfacial contact with hydrophilic probes.

Results suggest that the grafting-onto method is more prominent for the NCC, given the substrate's high surface area, which allows for more quaternisation over the surface and coverage by polymer grafts.

4 Conclusion

In this study, the authors have systematically explored how the grafting-onto protocol, specifically, the semi-dry kneading of cellulose with GTEAC, impacts the structural characteristics of two different types of cellulosic materials, i.e., MFC and NCC. The grafting-onto process introduces extensive structural and chemical modifications to the cellulose substrates, i.e., QMFC and QNCC, resulting in a total decrease in crystallinity, but keeping the crystalline domains intact, by increasing the amorphous content, enhancing moisture sorption capacity, and modifying thermal properties. The resulting structure-property relationships underscore the critical role of substrate morphology in dictating the performance of functionalised cellulosic materials. FTIR-ATR confirms successful quaternisation via emergence of C–N bands at ~1400 cm^{-1} and intensification of CH stretching modes (2979–2890 cm^{-1}). Structural analyses confirmed that the grafting mechanism primarily influences the amorphous domains and interfacial regions, inducing notable reductions in total crystallinity, from 85% (MFC) to 54% for QMFC and from 82% (NCC) to 60% for QNCC. Moreover, there are substantial modifications in microstructural parameters such as intercrystallite spacing D, i.e., from 4.3 nm (MFC) to 5.8 nm for QMFC and from 3.7 nm (NCC) to 5.0 nm for QNCC. Similarly, the correlation lengths ξ increase from 3.6 nm (MFC) to 5.5 nm (QMFC) and from 4.4 nm (NCC) to 4.7 nm (QNCC).

Thermal analyses revealed that grafted cellulosic materials exhibit reduced thermal stability due to the presence of thermolabile amorphous cationic polymer chains, which facilitate early-stage decomposition processes. For instance, TGA and DSC analyses reveal lowered onset and maximum peak decomposition temperatures, T_{on} and T_{max}, for grafted samples, i.e., QMFC (133 and 340 °C) and QNCC (142 and 288 °C), compared to the pre-grafted cellulosic materials, i.e., MFC (283 and 355 °C) and NCC (281 and 302 °C), respectively.

Equilibrium moisture contents at a_w = 0.95 increase from 18% (MFC) to 41% (QMFC), and from 26% (NCC) to 40% (QNCC). Analysis of the moisture sorption isotherms indicates an increase in the monolayer moisture content (MC_0) from 2.7 mmol/g (MFC) to 4.3 mmol/g (QMFC) and from 2.9 mmol/g (NCC) to 5.8 mmol/g (QNCC) with the corresponding increase in the specific surface area. Moreover, the near-unity hysteresis factor ($\eta \approx 1$) in grafted samples signifies highly reversible sorption, a direct consequence of the homogeneous cationic brush architecture.

The distinct differences observed between QMFC and QNCC, especially in terms of grafting efficiency, structural transformation, and sorptive performance, emphasise the crucial role of initial substrate morphology and surface area. QNCC, with its higher surface-to-volume ratio, showed more effective and homogeneous functionalisation, leading to superior water retention and interfacial interaction capabilities. These results collectively highlight the efficacy and versatility of the grafting-onto strategy using RILs. This could prove pivotal for developing a class of ionic IL-grafted biomaterials whose properties can be rationally engineered through processing.

The continued development of this platform has the potential to address pressing global needs in sustainable materials, clean water technologies, and biointerface engineering. Possible modifications to our established cellulose quaternisation process using GTEAC could focus on the substrate/template itself. This can allow for property control via selecting specific templates or architectures with differing accessible surface area, internal transport pathways; and mechanical integrity. Subsequently, this allows for a controlled variation in charge-site density, softness, hydrophilicity, thermal degradability and ionic capacity. Thus, substrate choice is an inherent 'knob' to the functionalisation process design. Points of use for such modifications can involve: (i) decentralised/small-scale water purification and ion removal (toxic anion scavenging); (ii) humidity buffering and moisture regulation (in packaging, biobased liners and humidity stabilisers); (iii) potential for contact-active antimicrobial behaviour at aqueous interfaces, (iv) potential for blue energy technologies where alternating cationic and anionic membranes harvest electrical potential from seawater vs. freshwater streams. Across all these points of use, cost reduction and the use of sustainable natural resources in materials design are the most evident objectives.

Acknowledgements
The authors would like to acknowledge the contributions of Anja Vieler from the Microscopy Lab at the Wood Research Institute of Munich (HFM) for the technical assistance with the SEM/EDX characterisation.

Author contributions
M.J.A. and A.S.F designed the experiments; M.J.A., B.W. and A.S.F. conducted the experiments; M.J.A. and A.S.F contributed to data analysis and manuscript writing, review, and editing; A.S.F. supervised the research; All authors reviewed the manuscript.

Funding
Open Access funding enabled and organized by Projekt DEAL. There was no Funding.

Data availability
Data has been disclosed herein in its entirety and is available upon request.

Declarations

Ethics approval and consent to participate
Not applicable.

Consent for publication
Not applicable.

Competing interests
The authors declare no competing interests.

Received: 19 July 2025 / Accepted: 29 December 2025
Published online: 05 January 2026

References

1. Joshi G, Rana V, Malik S, Bachheti RK. Assessment of different reaction media for the facile synthesis of cellulose-derived biorenewable polymer cationic cellulose: synthesis, characterization, and perspectives. ACS Omega. 2025;10:12476–86. https://doi.org/10.1021/acsomega.5c00044.
2. Ahmed MJ, Ashfaq J, Sohail Z, et al. Lignocellulosic bioplastics in sustainable packaging – recent developments in materials design and processing: a comprehensive review. Sustain Mater Technol. 2024;e01077. https://doi.org/10.1016/j.susmat.2024.e01077.
3. Barhoum A, Deshmukh K, García-Betancourt ML, et al. Nanocelluloses as sustainable membrane materials for separation and filtration technologies: principles, opportunities, and challenges. Carbohydr Polym. 2023;317:121057. https://doi.org/10.1016/j.carbpol.2023.121057.
4. Tedeschi G, Guzman-Puyol S, Paul UC, et al. Thermoplastic cellulose acetate oleate films with high barrier properties and ductile behaviour. Chem Eng J. 2018;348:840–9. https://doi.org/10.1016/J.CEJ.2018.05.031.
5. Koppolu R, Lahti J, Abitbol T, et al. Tailoring the performance of nanocellulose-based multilayer-barrier paperboard using biodegradable-thermoplastics, pigments, and plasticizers. Cellulose. 2023;30:6945–58. https://doi.org/10.1007/s10570-023-05281-x.
6. Kumar R, Sharma RK, Singh AP. Grafted cellulose: a bio-based polymer for durable applications. Polym Bull. 2018;75:2213–42. https://doi.org/10.1007/s00289-017-2136-6.

7. Ahmed MJ, Wu B, Sánchez-Ferrer A. Anion exchangers prepared from graft polymerisation of microfibrillated cellulose using the reactive ionic liquid. J Bioresources Bioprod. 2025;10:310–24. https://doi.org/10.1016/j.jobab.2025.04.001.
8. Ahmed MJ, Sánchez-Ferrer A. Wood-supported cationic polyelectrolyte membranes from a reactive ionic liquid for water detoxification. Chem Eng J. 2025;505:158841. https://doi.org/10.1016/j.cej.2024.158841.
9. Szabó L, Milotskyi R, Sharma G, Takahashi K. Cellulose processing in ionic liquids from a materials science perspective: turning a versatile biopolymer into the cornerstone of our sustainable future. Green Chem. 2023;25:5338–89. https://doi.org/10.1039/D2GC04730F.
10. Chowdhury S, Mohan RS, Scott JL. Reactivity of ionic liquids. Tetrahedron. 2007;63:2363–89. https://doi.org/10.1016/j.tet.2006.11.001.
11. Bodachivskyi I, Page CJ, Kuzhiumparambil U, et al. Dissolution of cellulose: are ionic liquids innocent or noninnocent solvents? ACS Sustain Chem Eng. 2020;8:10142–50. https://doi.org/10.1021/acssuschemeng.0c02204.
12. Missoum K, Belgacem MN, Barnes J-P, et al. Nanofibrillated cellulose surface grafting in ionic liquid. Soft Matter. 2012;8:8338. https://doi.org/10.1039/c2sm25691f.
13. Zhang C, Liu R, Xiang J, et al. Dissolution mechanism of cellulose in N,N -dimethylacetamide/lithium chloride: revisiting through molecular interactions. J Phys Chem B. 2014;118:9507–14. https://doi.org/10.1021/jp506013c.
14. Wang L, Hu J, Liu Y, et al. Ionic liquids grafted cellulose nanocrystals for High-Strength and toughness PVA nanocomposite. ACS Appl Mater Interfaces. 2020;12:38796–804. https://doi.org/10.1021/acsami.0c11217.
15. Zhang W, Yang G, Deng F, et al. Direct grafting of cellulose nanocrystals with poly(ionic liquids) via gamma-ray irradiation and their utilization for adsorptive removal of CR. Int J Biol Macromol. 2022;194:1029–37. https://doi.org/10.1016/j.ijbiomac.2021.11.175.
16. Livi S, Baudoux J, Gérard J-F, Duchet-Rumeau J. Ionic liquids: a versatile platform for the design of a multifunctional epoxy networks 2.0 generation. Prog Polym Sci. 2022;132:101581. https://doi.org/10.1016/j.progpolymsci.2022.101581.
17. Eftekhari A, Saito T. Synthesis and properties of polymerized ionic liquids. Eur Polym J. 2017;90:245–72. https://doi.org/10.1016/j.eurpolymj.2017.03.033.
18. Sehaqui H, Mautner A, de Perez Larraya U, et al. Cationic cellulose nanofibers from waste pulp residues and their nitrate, fluoride, sulphate and phosphate adsorption properties. Carbohydr Polym. 2016;135:334–40. https://doi.org/10.1016/j.carbpol.2015.08.091.
19. Chen G, Li T, Chen C, et al. A highly conductive cationic wood membrane. Adv Funct Mater. 2019;29:1902772. https://doi.org/10.1002/adfm.201902772.
20. Song Y, Sun Y, Zhang X, et al. Homogeneous quaternization of cellulose in NaOH/Urea aqueous solutions as gene carriers. Biomacromolecules. 2008;9:2259–64. https://doi.org/10.1021/bm800429a.
21. Naim MM, Batouti M El, Elewa MM. Novel heterogeneous cellulose-based ion-exchange membranes for electrodialysis. Polym Bull. 2022;79:9753–77. https://doi.org/10.1007/s00289-021-03978-2.
22. Hasani M, Cranston ED, Westman G, Gray DG. Cationic surface functionalization of cellulose nanocrystals. Soft Matter. 2008;4:2238–44. https://doi.org/10.1039/B806789A.
23. Zaman M, Xiao H, Chibante F, Ni Y. Synthesis and characterization of cationically modified nanocrystalline cellulose. Carbohydr Polym. 2012;89:163–70. https://doi.org/10.1016/j.carbpol.2012.02.066.
24. Hubbe MA, Rojas OJ, Lucia LA, Sain M. Cellulosic nanocomposites. A review. BioResources. 2008;3:929–80. https://doi.org/10.15376/biores.3.3.929-980.
25. Arcari M, Zuccarella E, Axelrod R, et al. Nanostructural properties and twist periodicity of cellulose nanofibrils with variable charge density. Biomacromolecules. 2019;20:1288–96. https://doi.org/10.1021/acs.biomac.8b01706.
26. Bertsch P, Sánchez-Ferrer A, Bagnani M, et al. Ion-induced formation of nanocrystalline cellulose colloidal glasses containing nematic domains. Langmuir. 2019;35:4117–24. https://doi.org/10.1021/acs.langmuir.9b00281.
27. Scheuchzer P, Zimmerman MB, Zeder C, et al. Higher extrusion temperature induces greater formation of less digestible type V and retrograded starch in iron-fortified rice grains but does not affect iron bioavailability: stable isotope studies in young women. J Nutr. 2022;152:1220–7. https://doi.org/10.1093/jn/nxab435.
28. Engelhardt M, Gilg HA, Richter K, Sanchez-Ferrer A. Adhesion-related properties of silver Birch (*Betula pendula* Roth) wood as affected by hydrophilic extraction. Wood Sci Technol. 2024;58:379–402. https://doi.org/10.1007/s00226-023-01526-x.
29. Sánchez-Ferrer A, Engelhardt M, Richter K. Anisotropic wood–water interactions determined by gravimetric vapor sorption experiments. Cellulose. 2023;30:3869–85. https://doi.org/10.1007/s10570-023-05093-z.
30. Berthold J, Rinaudo M, Salmeń L. Association of water to Polar groups; estimations by an adsorption model for lignocellulosic materials. Colloids Surf Physicochem Eng Asp. 1996;112:117–29. https://doi.org/10.1016/0927-7757(95)03419-6.
31. Viollaz PE, Rovedo CO. Equilibrium sorption isotherms and thermodynamic properties of starch and gluten. J Food Eng. 1999;40:287–92. https://doi.org/10.1016/S0260-8774(99)00066-7.
32. Willems W. The water vapor sorption mechanism and its hysteresis in wood: the water/void mixture postulate. Wood Sci Technol. 2014;48:499–518. https://doi.org/10.1007/s00226-014-0617-4.
33. Willems W. A critical review of the multilayer sorption models and comparison with the sorption site occupancy (SSO) model for wood moisture sorption isotherm analysis. Holzforschung. 2015;69:67–75. https://doi.org/10.1515/hf-2014-0069.
34. Seddiqi H, Oliaei E, Honarkar H, et al. Cellulose and its derivatives: towards biomedical applications. Cellulose. 2021;28:1893–931. https://doi.org/10.1007/s10570-020-03674-w.
35. Kljun A, Benians TAS, Goubet F, et al. Comparative analysis of crystallinity changes in cellulose I polymers using ATR-FTIR, X-ray diffraction, and carbohydrate-binding module probes. Biomacromolecules. 2011;12:4121–6. https://doi.org/10.1021/bm201176m.
36. Kopač T, Krajnc M, Ručigaj A. A rheological study of cationic micro- and nanofibrillated cellulose: quaternization reaction optimization and fibril characteristic effects. Cellulose. 2022;29:1435–50. https://doi.org/10.1007/s10570-021-04365-w.
37. Szcześniak L, Rachocki A, Tritt-Goc J. Glass transition temperature and thermal decomposition of cellulose powder. Cellulose. 2008;15:445–51. https://doi.org/10.1007/s10570-007-9192-2.
38. Wu J, Du X, Yin Z, et al. Preparation and characterization of cellulose nanofibrils from coconut coir fibers and their reinforcements in biodegradable composite films. Carbohydr Polym. 2019;211:49–56. https://doi.org/10.1016/J.CARBPOL.2019.01.093.

39. Alharthi S, Grishkewich N, Berry RM, Tam KC. Functional cellulose nanocrystals containing cationic and thermo-responsive polymer brushes. Carbohydr Polym. 2020;246:116651. https://doi.org/10.1016/j.carbpol.2020.116651.
40. Fu X, Yang Q, Zhang Y. Thermal decomposition behavior and mechanism study of cationic polyacrylamide. J Therm Anal Calorim. 2021;146:1371–81. https://doi.org/10.1007/s10973-020-10131-0.
41. Belbekhouche S, Bras J, Siqueira G, et al. Water sorption behavior and gas barrier properties of cellulose whiskers and microfibrils films. Carbohydr Polym. 2011;83:1740–8. https://doi.org/10.1016/j.carbpol.2010.10.036.
42. Soidinsalo O, Opstad A, Øvrebø HH. Improved barrier performance of water-based barrier coatings with microfibrillated cellulose. TAPPI J. 2025;24:142–50. https://doi.org/10.32964/TJ24.3.142.
43. Fotie G, Gazzotti S, Ortenzi MA, et al. Performance comparison of coatings based on cellulose nanocrystals and microfibrillated cellulose for food packaging. Carbohydrate Polymer Technologies and Applications. 2023;5:100264. https://doi.org/10.1016/j.carpta.2022.100264.
44. Hou S, Wang J, Yin F, et al. Moisture sorption isotherms and hysteresis of cellulose, hemicelluloses and lignin isolated from birch wood and their effects on wood hygroscopicity. Wood Sci Technol. 2022;56:1087–102. https://doi.org/10.1007/s00226-022-01393-y.
45. Sánchez-Ferrer A, Engelhardt M. Determination of the water diffusivity dependence with the flow rate using a DVS equipment. Eur J Wood Wood Prod. 2025;83:24. https://doi.org/10.1007/s00107-024-02182-z.
46. Harrisson S, Drisko GL, Malmström E, et al. Hybrid rigid/soft and biologic/synthetic materials: polymers grafted onto cellulose microcrystals. Biomacromolecules. 2011;12:1214–23. https://doi.org/10.1021/bm101506j.
47. Roy D, Guthrie JT, Perrier S. Graft polymerization: grafting poly(styrene) from cellulose via reversible addition – fragmentation chain transfer (RAFT) polymerization. Macromolecules. 2005;38:10363–72. https://doi.org/10.1021/ma0515026.
48. Zhang X, Zhu W, Guo J, et al. Impacts of degree of substitution of quaternary cellulose on the strength improvement of fiber networks. Int J Biol Macromol. 2021;181:41–4. https://doi.org/10.1016/j.ijbiomac.2021.03.121.

Publisher's note